

# Phase Transitions in Cellulose Microfibril Dispersions by High-Energy Mechanical Deagglomeration

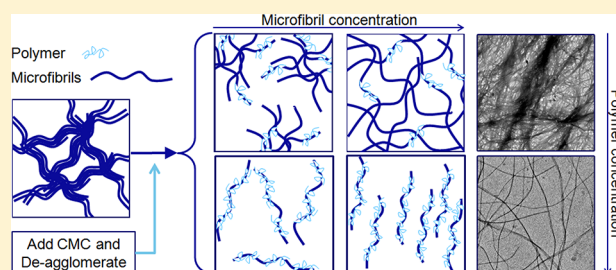
Sandra J. Veen,<sup>\*,†</sup> Anke Kuijk,<sup>†</sup> Peter Versluis,<sup>†</sup> Henk Husken,<sup>†</sup> and Krassimir P. Velikov<sup>\*,†,‡</sup>

<sup>†</sup>Unilever Research Vlaardingen, Olivier van Noortlaan 120, 3133 AT Vlaardingen, Netherlands

<sup>‡</sup>Soft Condensed Matter, Debye Institute for Nanomaterials Science, Department of Physics and Astronomy, Utrecht University, Princetonplein 1, 3584 CC Utrecht, Netherlands

## Supporting Information

**ABSTRACT:** It is shown that dispersions of cellulose microfibrils display gel–sol and direct gel–colloidal liquid crystalline structure transitions. This is achieved by applying high-energy mechanical deagglomeration to bacterial cellulose (BC) networks in the presence of sodium carboxymethyl cellulose (CMC). At high CMC content adsorption of the polymer leads to a significant increase in the  $\zeta$  potential. The resulting apparent phase diagram shows transitions from aggregates to single microfibril dispersions with increasing the CMC/BC weight ratio at low microfibril concentrations. At higher concentrations, liquid crystalline ordering was observed and the microstructure becomes more homogeneous with increasing the CMC content. The observed liquid crystalline ordering was found to be reminiscent of nematic gels. Applying deagglomeration in the presence of CMC, thus, transitions the system from aggregates and gels to dispersions of single microfibrils and nematic gel-type structures.



## INTRODUCTION

Colloidal systems can transition from equilibrium phases to non-equilibrium structures by means of the sol–gel transition: a transition from a stable colloidal dispersion (sol) to an arrested network (gel). This can be achieved by, for instance, increasing the concentration of colloids or creating attraction between the particles.<sup>1</sup> Several industrially important materials, such as clays, carbon nanotubes, and cellulose microfibrils (CMFs), however, are produced or found in nature in a highly aggregated state.<sup>2–4</sup> To create stable dispersions and study the phase behavior of these materials, one first needs to deagglomerate the system. In essence, the reverse transition needs to be applied: from a gel to a sol. At high volume fractions, dependent upon the particle shape and interactions, even more complex transitions to, for instance, more ordered phases could be expected. The deagglomeration of these systems is thus critical for their understanding.

Cellulose is an important natural material used in many industrial applications.<sup>5</sup> Cellulose particles can, depending upon its source or chemical treatment, be considered as either rod-like or semi-flexible. For suspensions with rod-like particles, such as charged cellulose whiskers,<sup>6</sup> the phase behavior is widely studied and several different structures can be formed depending upon the rod aspect ratio and volume fraction. These structures can range from system-spanning (percolating) networks to nematic and smectic colloidal liquid crystals and even cholesteric phases.<sup>7</sup> The rich phase behavior of semi-flexible fibrillar systems, however, is not yet fully understood,<sup>8</sup>

and a complete theoretical description is still lacking.<sup>9,10</sup> This holds especially for transitions from gels to crystalline states.

Bacteria of the strain Aceto Bacter form a very pure form of cellulose in the form of ribbon-shaped microfibrils (~60 nm wide, ~9 nm thick, and up to several micrometers long) by building up the polysaccharides from the glucose molecules that they consume.<sup>11</sup> After their formation, however, the CMFs agglomerate into space-filling networks. The agglomeration is driven by surface OH-group-mediated hydrogen bonds and van der Waals attractions. High-energy mechanical treatment can separate the network into individual microfibrils, but because of their attractive nature, they readily aggregate again or form gels.<sup>12</sup> The presence of the OH groups does result in a low amount of surface charge ( $\zeta$  potential of  $-7.5$  mV<sup>13</sup>), but this is not enough to stabilize the microfibrils. The systematic study of the CMF phase behavior therefore requires control of the interactions between the microfibrils.

Aggregation of the CMFs can be prevented by adding charge to the cellulose surface, for instance, by chemical surface modification<sup>14,15</sup> or by adding an adsorbing polymer.<sup>16</sup> The charged polymer carboxymethyl cellulose (CMC) is well-known for its affinity for cellulose surfaces.<sup>17,18</sup> The addition of adsorbing polymers (e.g., CMC) during high-energy mechanical deagglomeration, however, has not been studied before, especially the combination of high shear rates ( $\sim 10^7$  s<sup>-1</sup>) and

Received: April 2, 2014

Revised: October 8, 2014

Published: October 14, 2014

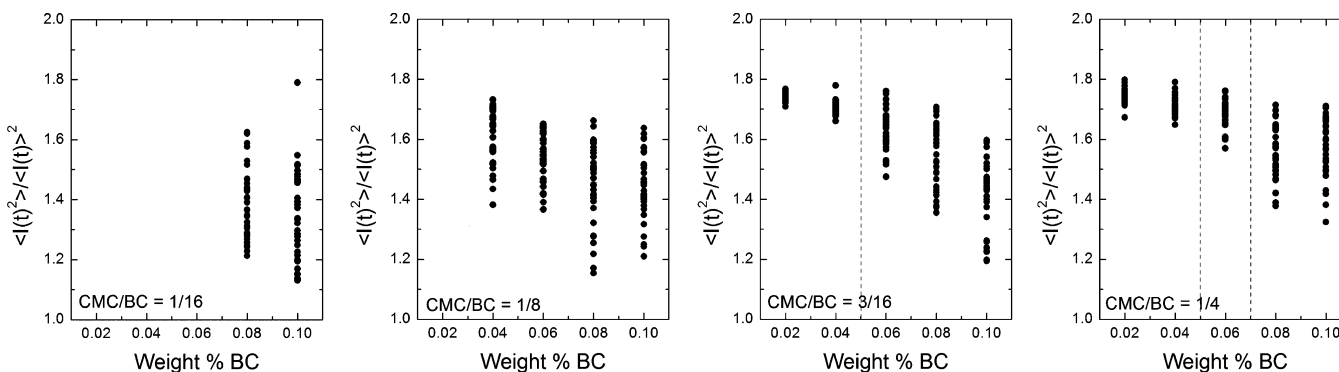


**Figure 1.**  $\langle I(t)^2 \rangle / \langle I(t) \rangle^2$  as a function of the CMC concentration for four different weight ratios of CMC/BC recorded at different positions in the sample.

an adsorbing polymer as a means to individualize CMFs to control their phase behavior. Here, it is shown that, using this approach, the phase behavior gradually changes from aggregates and gels to CMC dispersions and colloidal liquid crystal-type structures.

## EXPERIMENTAL SECTION

Cubes of bacterial cellulose (BC) in syrup from eight plastic cups with 220 mL of lychee/vanilla flavored nata de coco dessert (Kara Santan Pertama, Bogor 16964, Indonesia) were immersed in 1.5 L of nanopure water (Barnstead Nanopure Diamond, resistance of 18 M $\Omega$  cm). The cubes were then cut using a hand blender (Braun 4185545) and washed. Each washing step consisted of rinsing the cellulose by filtration over a vacuum filter (Whatman Schleicher and Schuell 113, wet-strengthened circles, 185 mm in diameter) and redispersing the residue in 1.5 L of nanopure water with the hand blender. After 8 washing steps, the cellulose residue was redispersed in 400 mL of nanopure water. The weight percentage (wt %) of BC in the resulting suspension was determined by a moisture analyzer (HB43-S Mettler Toledo). Mixtures of BC and CMC were prepared by adding different amounts of CMC [Ashland Blanose Aqualon, 99.5% pure, 9M31XF,  $M_w \approx 250\,000$  g/mol, degree of polymerization of 1100, degree of substitution (DS) of the carboxymethyl groups of 0.8–0.95] and nanopure water and mixing with a Sylverson mixer (L4RTA) for 5 min at 3600 rpm. These samples were passed once through a Microfluidizer (M110S, Microfluidics) with a  $z$  chamber of 87  $\mu\text{m}$  at a pressure of 1200 bar. Dilutions were made from the obtained stock solutions by dilution with nanopure water.

Dynamic light scattering (DLS) and mobility measurements were performed on a Malvern Zetasizer Nano ZS at 20  $^\circ\text{C}$ . DLS was performed with a 633 nm laser at a backscattering angle of 173 $^\circ$  imposed by the Zetasizer configuration. At least four independent measurements were performed at nine different positions in the sample by choosing different horizontal positions in the cuvette. The coherence factor of the setup was 0.82, determined with a calibration sample containing polystyrene spheres of 356 nm (Polyscience, Inc., Polybead). The operation limits for the mobility measurements are  $> \pm 20 \mu\text{m cm V}^{-1} \text{s}^{-1}$  for the particle mobility and  $> \pm 500$  mV for the  $\zeta$  potential.

Confocal microscopy was performed on a Leica TCS-SP5. For staining, 1 drop of 0.5% Congo Red solution in water was added to 1 mL of dispersion. For imaging, the samples were placed between two coverslips separated by a (3 mm) spacer. Transmission electron microscopy (TEM) was performed on a Tecnai20 system from FEI. A drop of dispersion was placed on a carbon only 300 mesh copper TEM grid (Agar Scientific), of which the surface was made hydrophilic by glow discharge. Excess solvent was blotted away with a small filter paper, after which the samples were negatively stained by adding a drop of phosphotungsten acid (2%, w/v) in water onto the grid. Excess liquid was blotted with a small filter paper, after which the samples were left to dry in air before imaging.

Viscosity measurements of the continuous phase were performed to determine the amount of adsorbed CMC.<sup>19</sup> The continuous phase was obtained by centrifugation of the CMC/BC dispersions in a Heraeus Biofuge Primo R for 4.75 h at a speed of 13 000 rpm at a temperature of 20  $^\circ\text{C}$ . Viscosity measurements were performed on an Anton Paar Physica MCR301 rheometer, using a plate–plate geometry (plate diameter of 25 mm and gap of 0.1 mm). The zero shear viscosity at 20  $^\circ\text{C}$  was determined by increasing the shear rate from 100 to  $1 \times 10^5$   $\text{s}^{-1}$ . A calibration curve of viscosity as a function of the CMC concentration was constructed from a CMC solution of 0.2 wt %, passed once through the Microfluidizer with a  $z$  chamber of 87  $\mu\text{m}$  at a pressure of 1200 bar.

## RESULTS AND DISCUSSION

The effect of the presence of CMC during high-energy mechanical deagglomeration of BC networks was tested by comparing four different CMC/BC weight ratios, namely, 1:16, 1:8, 3:16, and 1:4, and pure BC. Five different concentrations from 0.02 to 0.1 wt % were investigated. The phase behavior of these suspensions was investigated with the help of DLS. To distinguish between dispersions and arrested states, such as gels,<sup>20,21</sup> the normalized intensity correlation function given by  $g^{(2)}(\tau) = \langle I(t)I(t+\tau) \rangle / \langle I(t) \rangle^2$  was measured. Here,  $I(t)$  and  $I(t+\tau)$  are the scattering intensity at time  $t$  and  $t+\tau$ , respectively. The brackets indicate a time-averaged value. For a dispersion of freely diffusing particles,  $g^{(2)}(\tau)$  will theoretically begin at its intercept at 2 and decay to 1.<sup>20</sup> When a system is arrested in a gel,  $g^{(2)}(\tau)$  will no longer decay to 1 but to a fixed higher plateau value. The ratio of the intercept over the plateau value or the normalized second moment of the scattering intensity  $\langle I(t)^2 \rangle / \langle I(t) \rangle^2$ , thus, offers a simple way to distinguish between the two cases: for a dispersion, its value will be close to 2 and will not change with measurement position, but for an arrested state, it will be lower than 2 and change depending upon the measurement position. Because of the large surface area of the detector, the intercept will in practice at most be equal to the coherence factor + 1, which for the setup used is 1.82.<sup>22</sup> The  $\langle I(t)^2 \rangle / \langle I(t) \rangle^2$  for stable samples of concentration series of BC at the different CMC/BC ratios is shown in Figure 1. A sample was considered stable when no sedimentation was detected over the course of a complete light-scattering experiment ( $\sim 2$  h).

For the DLS measurements, five different concentrations of BC were investigated per CMC/BC ratio, ranging from 0.02 to 0.1 wt %. Suspensions containing only BC could not be measured with DLS because sedimentation occurred within minutes after preparing the samples. The unmodified microfibrils readily aggregate and sediment to form a self-supporting

network.<sup>12</sup> For the lowest CMC/BC ratio (1:16), samples with low BC concentrations also showed sedimentation. Increasing the CMC content improved the stability of the samples. Sedimentation reduced, allowing for the measurement of samples of lower volume fraction of CMF at higher CMC/BC ratios.

For those samples that did remain stable, two different types of scattering behavior could be distinguished. As seen from Figure 1 for CMC/BC ratios of 1:16 and 1:8,  $\langle I(t)^2 \rangle / \langle I(t) \rangle^2$  was considerably lower than 1.82 and greatly dependent upon the measurement position, illustrated by the large spread in values. This behavior is typical for an arrested state. At CMC/BC ratios of 3:16 and 1:4, however, a transition can be seen. At low BC concentrations, the spread in  $\langle I(t)^2 \rangle / \langle I(t) \rangle^2$  is small and values are close to 1.82. This indicates a dispersion in which the microfibrils are free to diffuse through the system. This is supported by the presence of single microfibrils in TEM images of the same samples (see Figure S1 of the Supporting Information). Upon increase of the BC concentration, there is a clear transition in which the spread in  $\langle I(t)^2 \rangle / \langle I(t) \rangle^2$  suddenly increases. This indicates a transition from a dispersion (sol) to an arrested state (lines in Figure 1).

Time is a big factor when it comes to the stability of the CMC/BC suspensions. The presence of small amounts of CMC during deagglomeration increases the time frame over which aggregation and sedimentation occurs but does not prevent the process completely, because cellulose has a relatively large density (1.5 g/mL). Some samples that remained stable during the DLS measurement did display sedimentation over the course of 4 days (see Figure 2). Samples containing 0.06 wt % BC and higher at CMC/BC of

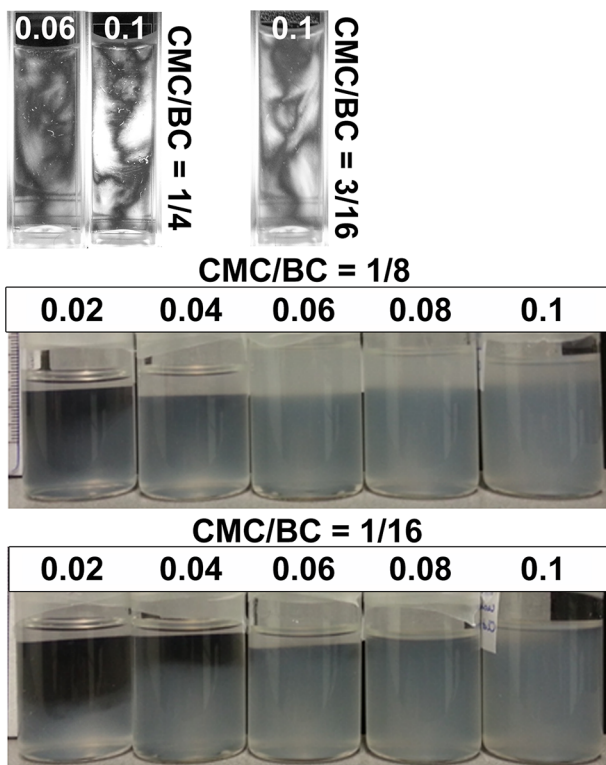


**Figure 2.** (Top) Microfibril dispersions in 1 cm cuvettes between crossed polarizers. Clear macroscopic liquid crystalline domains can be seen for the high CMC/BC ratios. (Bottom) Sedimentation in BC dispersions after 4 days for the low CMC/BC ratios.

1:8, however, did not show any sedimentation. This, together with the large spread in  $\langle I(t)^2 \rangle / \langle I(t) \rangle^2$ , indicates that a system-spanning gel is formed.

At higher CMC/BC ratios, the microfibril dispersions change their phase behavior dramatically. Although CMC/BC of 1:4 and 3:16 form stable dispersions at low concentrations, at higher concentrations, the DLS results clearly point to an arrest in the movement of the microfibrils. These structures did not show any sign of sedimentation. When observed between crossed polarizers, it is clear that the resulting state is not a regular gel. Clear macroscopic light and dark domains give evidence of microfibril alignment (Figure 2).

Despite this clear alignment of the microfibrils for CMC/BC of 1:4 and 3:16, both light scattering as well as rheological measurements still reveal gel-like behavior at a BC concentration of 0.1 wt % (see Figure S2 of the Supporting Information). The solid character of the gels does decrease with increasing the CMC content, pointing to an increase in alignment of the microfibrils (see Figures S2 and S3 of the Supporting Information). The resulting state does not seem to be an equilibrium liquid crystal but shows similarities to a nematic gel. This type of gel closely resembles the nematic liquid crystal structure and is observed for several systems containing anisotropic particles, ranging from clay platelets to boehmite rods.<sup>23–27</sup>

A deviating scattering behavior was observed for the 0.06 wt % BC sample. A characteristic spread in  $\langle I(t)^2 \rangle / \langle I(t) \rangle^2$  was seen: most points were close together, with only a few small deviations to lower values. Between crossed polarizers, liquid-crystalline-structured domains could be seen but less pronounced than at higher BC concentrations. This behavior seems to be in between that of an arrested state and a dispersion. The complete apparent phase behavior of the CMC/BC system is summarized in Figure 3.

The light-scattering results as well as the macroscopic observations of the sedimentation point to clear differences in the microstructure of the CMF suspensions. Confocal images taken from samples containing 0.1 wt % BC at different CMC/BC ratios demonstrate that this is indeed the case (Figure 4). Qualitatively, the dispersions show less and smaller bundles of

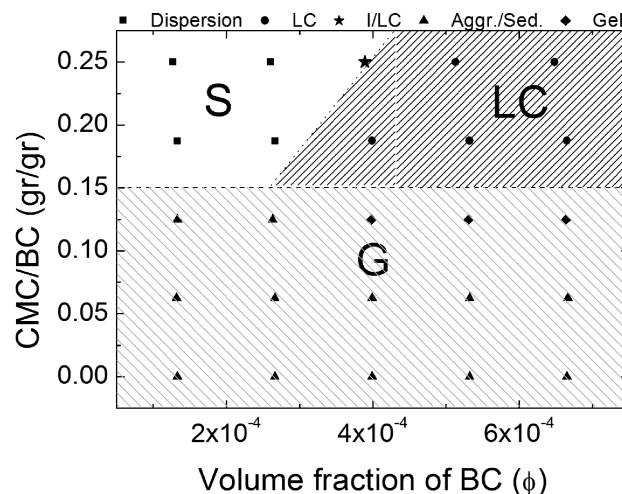


**Figure 3.** Apparent phase diagram of CMFs, deagglomerated in the presence of CMC. Dependent upon the concentrations and CMC/BC ratio, the system forms a dispersion [S (sol)], aggregates to form a network [G (gel)], or liquid crystalline structures (LC).

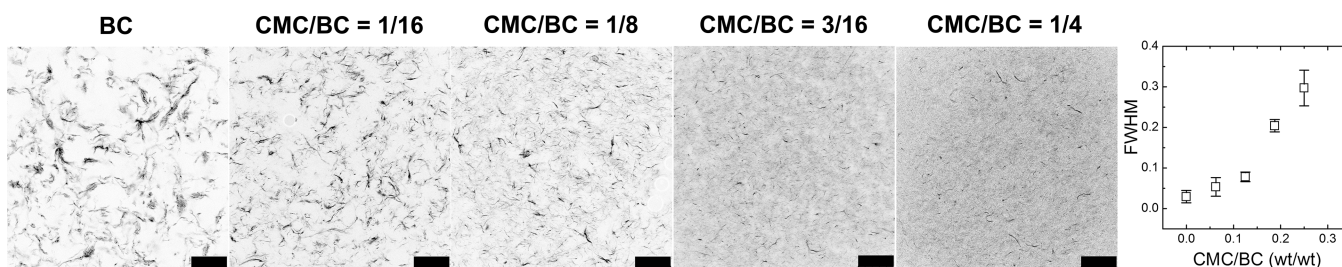


**Figure 4.** Distribution of the microfibrils in dispersions of 0.1 wt % BC. Scale bar = 250  $\mu\text{m}$ . Images are inverted: white, background; black to gray, fluorescence. fwhm of the normalized intensity distribution of the confocal images shown. Error bars are 3 times standard deviation (99.73% accuracy).

microfibrils and smaller voids between them as the CMC/BC ratio increases. In Figure 4, the full width at half maximum (fwhm) of the normalized intensity distribution of the confocal images shown, is plotted as a function of the CMC/BC ratio (for details, see the Supporting Information). The fwhm quantifies the spread of the microfibrils and, hence, gives a measure for the homogeneity of the sample. A value of 1 indicates a completely homogeneous spread. Increasing the amount of CMC in the system increases the value for the fwhm from 0.04 to 0.28, resulting in an improved homogeneity.

The ability of CMC to prevent reaggregation of the microfibrils after deagglomeration of the network is also evident from TEM images. Figure 5 shows images of samples

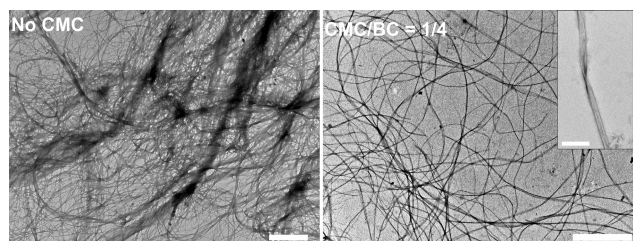


**Figure 5.** TEM images of the microfibrils treated with and without CMC (scale bar = 2  $\mu\text{m}$ ; 0.01 wt % BC). (Inset) Characteristic ribbon structure of CMFs (scale bar = 250 nm).

containing 0.01 wt % mechanically treated pure BC in water and at a CMC/BC ratio of 1:4. Even though the dispersions are dried before imaging, a clear difference is seen in the spread of the microfibrils. The pure BC microfibrils are present in large bundles and aggregates, while the CMC-containing microfibrils are homogeneously deposited on the grid. The ribbon shape and its semi-flexible nature are also clearly visible (inset with CMC/BC = 1:4 in Figure 5). The microfibrils have an average width of  $\sim 60$  nm and thickness of  $\sim 9$  nm. The length averages on 15  $\mu\text{m}$ , ranging from 2  $\mu\text{m}$  to as large as 40  $\mu\text{m}$ .

The addition of CMC to wood cellulose suspensions is known to disrupt flocs and induce better dispersion of cellulose fibers<sup>28</sup> and microfibrils.<sup>16</sup> In general, there are two mechanisms by which this can be achieved. One is by increasing the viscosity of the medium, under conditions in which CMC does not adsorb onto the cellulose surface.<sup>16,29</sup> The increased viscosity reduces the mobility of the particles and, thereby, the amount of hooks and bends between them. However, CMC does have a strong affinity for cellulose and can adsorb and even irreversibly attach if the conditions are favorable, leading to an increase in microfibril surface charge. For the charged particles obtained from wood cellulose, these conditions include a.o. solutions at low pH (<6) and high salt

concentrations.<sup>29–31</sup> From a colloidal perspective, this results in the lowering of the repulsive barrier in the interaction potential between the slightly negatively charged cellulose and the negatively charged CMC. The polymer can then more easily form multiple hydrogen bonds between its glucose backbone and the cellulose surface.

To see if adsorption of CMC is responsible for the observed changes in CMF phase behavior, the amount of adsorbed CMC needs to be known. The amount of free CMC after deagglomeration was therefore determined by measuring the viscosity of the continuous phase after removing the BC from suspensions by centrifugation<sup>19</sup> (see the Supporting Information). Any adsorption of the polymer would result in less free CMC than added before deagglomeration. The results show that this is indeed the case. The adsorption of CMC as a function of the CMC added before mechanical treatment is summarized in Figure 6. Dependent upon the CMC/BC ratio,

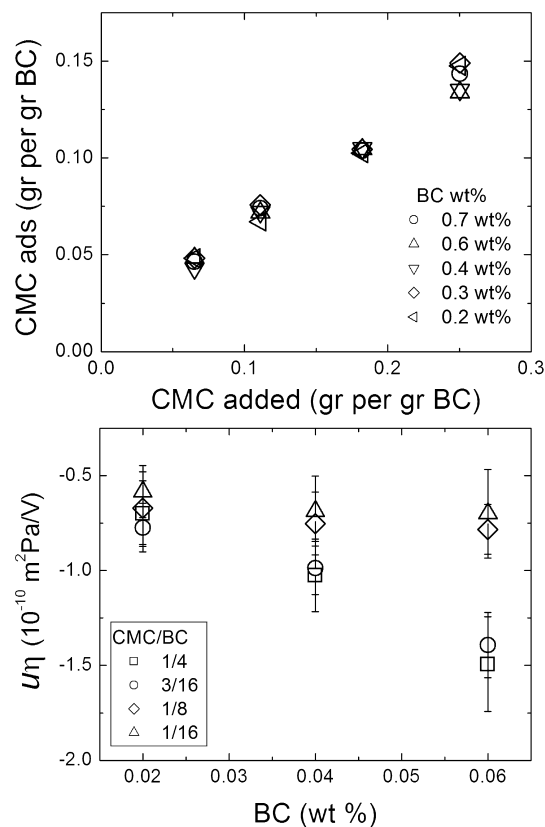


**Figure 6.** Adsorbed CMC and mobility times viscosity of the continuous phase of the CMC/BC dispersions.

55–75% of the CMC adsorbed onto the BC surface. Adding more CMC to the BC network during deagglomeration also results in more adsorption of CMC. Using the average microfibril dimensions and the maximum amount of carboxyl groups on the CMC polymer, the maximum bare surface charge density could be calculated from the measured CMC adsorption. This increased from  $\sim 0.65$  e/nm<sup>2</sup> at a CMC/BC ratio of 1:16,  $\sim 1.2$  e/nm<sup>2</sup> at a ratio of 1:8,  $\sim 1.6$  e/nm<sup>2</sup> at a ratio of 3:16, to  $\sim 2.1$  e/nm<sup>2</sup> at a ratio of 1:4. The actual surface charge density will probably be smaller because of counterion condensation<sup>32</sup> (see the Supporting Information).

In the system presented, the ionic strength is low ( $< 0.5$  mM) and the pH is close to 6. For charged CMF, these conditions would be unfavorable for adsorption. The surface charge on CMF from BC on the other hand is very low. Adsorption is therefore still favorable under the solution conditions used. However, for the CMC to completely cover the CMF surface and stabilize the individual microfibrils, the fibrils first need to be deagglomerated. Adding CMC to the microfibrils before or after deagglomeration, therefore, gives markedly different results. Where adding CMC before mechanical treatment stabilizes single microfibrils, adding CMC afterward leads to stabilization of a dispersion of flocs from microfibrils.<sup>16,33</sup> The presence of CMC during deagglomeration is thus key in obtaining individualized microfibrils.

To determine if the increase in CMC adsorption also leads to an increase in surface charge on the microfibrils, electrophoretic mobility measurements were performed by means of electrophoresis. The results are shown in Figure 6. Because of the presence of unbound CMC in the continuous phase, the viscosity differs from that of pure water. To compare the different measurements, the mobility ( $u$ ) is multiplied by the viscosity ( $\eta$ ) of the continuous phase. Overall, the measurements reveal negatively charged species in solution. At CMC/BC of 1:16 and 1:8, the mobility is independent of the BC concentration. At these ratios and BC concentrations, there are aggregates in solution. Because of their large size and open structure, no estimate could be made of their  $\zeta$  potential on the basis of their mobility.

For ratios of 3:16 and 1:4, the mobility increases with the BC concentration. Light scattering shows that, in these suspensions, the system contains single microfibrils and is moving closer to the point at which liquid crystalline structures are observed. It is thus possible that the particles no longer move isotropically. For rod-like particles, the mobility for isotropic movement is  $2/3$  of the mobility along the long axis of the rod.<sup>23</sup> The mobility increase seen between BC concentrations of 0.02 and 0.06 wt % is of this order of magnitude and could, therefore, be the result of a gradual alignment. The  $\zeta$  potential for the microfibrils can be estimated by taking the mobility at the lowest BC concentration and using the expression for infinitely long rods:  $u = 2\epsilon_0\epsilon_r\zeta/3\eta$  ( $\epsilon_0$  is the permittivity in vacuum and  $\epsilon_r$  is the relative permittivity of the solvent), which is valid for  $\kappa a < 1$ , in which  $a$  is the radius of the rod and  $\kappa$  is the inverse Debye screening length.<sup>23</sup> There is no additional salt added to the dispersion, and on the basis of the pH ( $\sim 6$ ) and added CMC, the Debye length was estimated to be on average  $\sim 40$  nm. The estimate for  $\zeta$  for CMC/BC of 1:4 and 3:16 at a concentration of 0.02 wt % was  $\sim -150$  mV, which is considerable higher than that for pure BC ( $-7.5$  mV<sup>13</sup>). This value is in close agreement with what is calculated for the surface potential of carboxymethylated high-pressure homogenized wood CMFs under similar solution conditions<sup>34,35</sup> and

measured for carboxylated cellulose nanocrystals<sup>36</sup> as well as for pure CMC of similar degree of substitution.<sup>37</sup> The charges on these particles originate from the same surface groups as the CMC-treated BC microfibrils.

The experimental results show that, at sufficiently high adsorption of CMC, the system shows structures reminiscent of the traditional isotropic (I)/nematic (N) phase transitions as seen, for instance, for boehmite rods, clay particles, vanadium oxide, and even cellulose nanowhiskers.<sup>8,25,27,38–41</sup> Although attractive rod-like particles can in theory form colloidal liquid crystal phases, these are often not observed because they are preceded by a gel phase.<sup>42</sup> This is also the case for the microfibrils. For equilibrium liquid crystals, the I/N phase transition can be described by Onsager's theory.<sup>43</sup> For hard rods, the volume fraction at which the I/N transition occurs depends upon the particle aspect ratio [length ( $L$ ) over diameter ( $D$ )]. The BC microfibrils are on average  $15 \mu\text{m}$  long and  $60$  nm wide. According to Onsager's theory, the expected I/N phase transition for hard rods of these dimensions lies at a volume fraction ( $\phi$ ) of  $\sim 2 \times 10^{-2}$ . The light scattering experiments show a transition from dispersion to liquid crystal-like alignment around a concentration of 0.06 wt %. When the density of the microfibrils is taken to be  $1.5$  g/mL,<sup>44</sup> this corresponds to a  $\phi$  of  $\sim 4 \times 10^{-4}$ . This transition is at least 2 orders of magnitude lower than the theoretical transition. The microfibrils, however, are negatively charged, in which case an effective size of the particle needs to be taken into account by adding the Debye screening length ( $\kappa^{-1}$ ) ( $\sim 40$  nm) to the dimensions of the particle. This results in an effective length of  $L + 2\kappa^{-1}$  and an effective diameter of  $D + 2\kappa^{-1}$ . The observed transition now lies at a  $\phi$  of  $0.9 \times 10^{-2}$ , which is only 1 order of magnitude lower than the theoretical transition.

Not only charge but also polydispersity of the microfibrils can lead to considerable changes in the I/N phase transition.<sup>10</sup> Longer microfibrils can dominate the I/N phase transition and shift it to lower  $\phi$ . TEM measurements show (see Figures S4 and S5 of the Supporting Information) that the polydispersity in length is considerable and microfibrils up to  $\sim 40 \mu\text{m}$  long can be found. Taking into account the largest aspect ratio of  $L/D \sim 650$  and the effective volume of the microfibrils because of  $\kappa^{-1}$ , the theoretical I/N phase transition now lies at  $\phi \sim 1.3 \times 10^{-2}$ , which is comparable to the experimentally observed transition (see Table S1 of the Supporting Information).

The TEM images suggest that the microfibrils are more semi-flexible rather than rod-like. In this case, it is the persistence length ( $l_p$ ) and not  $L$  that determines the I/N phase transition. For the microfibrils,  $l_p$  was determined to be  $\sim 11 \mu\text{m}$  from TEM images (see the Supporting Information). Using the analytical expressions for charged long semi-flexible polyelectrolytes,<sup>45</sup> this would give a theoretical I/N transition at  $\phi \sim 7 \times 10^{-2}$ . This is close to the calculated rod transition and, hence, to what is found for the microfibrils.

Although the observed I/N transitions and the predicted value for the microfibrils are similar, the observed structures are not necessarily equilibrium structures. In comparable systems, I/N phase coexistence can be observed within hours to days. Complete equilibrium may not be reached after years.<sup>46</sup> At high concentrations, where nematic-type ordering does take place, the CMC/BC suspensions still show gel-like characteristics, which indicate the existence of a nematic gel. Nematic gels usually occur at volume fractions higher than the I/N phase transition in systems that do show I/N coexistence.<sup>47</sup> The CMC/BC dispersions do not show I/N phase separation. This

may point to another possible colloidal liquid crystalline structure: liquid crystalline domains embedded in a microfibril gel.

These structures may be the result of the deagglomeration pathway taken in the preparation of the dispersions, in which the system is changed from a gel of attractive particles to a repulsive system at high CMC/BC ratios. This is opposite from traditional colloidal systems, in which stable dispersions are destabilized to form a gel by adding salt or changing the pH. In the method employed here, interactions are not changed by screening of the surface charges or altering the dissociation of the surface groups. Instead, the amount of available surface groups is actively changed by adsorbing more or less CMC onto the microfibril surface. As already mentioned, chemical modification of the cellulose surface can introduce a similar effect. However, mechanical treatment still needs to be applied along with centrifugation to remove aggregates.<sup>14,15,48,49</sup> The method applied here offers a one-step route to the alteration of the surface properties and, hence, the interactions between the microfibrils. Another advantage is that, unlike the rod-like cellulose nanowhiskers, where acid hydrolysis breaks the larger cellulose fibers into their crystalline parts, the mechanical treatment retains the intrinsically ribbon-like structure and the large aspect ratio of the microfibrils.

## CONCLUSION

Mechanical deagglomeration of networks of BC in the presence of CMC results in gel–sol and direct gel–liquid crystalline structure transitions in the obtained microfibril dispersions. The observed increase in CMC adsorption with increasing the CMC concentration leads to more homogeneous microstructures and a significant increase in the  $\zeta$  potential of the microfibrils, preventing reaggregation and resulting in the formation of colloidal liquid crystalline structures. The benefit of this system is that the bare surface charge density can be gradually changed by the adsorption of different amounts of CMC and, hence, offers control over the colloidal interactions. The results presented are important in understanding the formation of liquid crystals by charged semi-flexible polymers and may offer new insight into the underlying theory of their phase behavior. Finally, these insights can help in the understanding and use of other fibrillar materials (e.g., protein fibrils and carbon nanotubes).

## ASSOCIATED CONTENT

### Supporting Information

TEM images of single CMFs of a BC dispersion deagglomerated in the presence of CMC, rheological properties of CMC/BC dispersions at different CMC/BC weight ratios, photographs taken of a CMC/BC and pure BC dispersion to illustrate flow, details on confocal image analysis, details on CMC adsorption measurements, calculations of counterion condensation on the microfibrils, dimensions of BC fibers as measured by TEM, and calculations of the I/N phase transition. This material is available free of charge via the Internet at <http://pubs.acs.org>.

## AUTHOR INFORMATION

### Corresponding Authors

\*E-mail: [sandra.veen@unilever.com](mailto:sandra.veen@unilever.com).

\*E-mail: [krassimir.velikov@unilever.com](mailto:krassimir.velikov@unilever.com).

## Notes

The authors declare no competing financial interest.

## ACKNOWLEDGMENTS

This research was financially supported by NanoNextNL (a consortium of the Dutch government and 130 other partners).

## REFERENCES

- (1) Anderson, V. J.; Lekkerkerker, H. N. W. Insight into phase transitions kinetics from colloid science. *Nature* **2002**, *416*, 811–815.
- (2) Vigolo, B.; Coulon, C.; Maugey, M.; Zakri, C.; Poulin, P. An experimental approach to the percolation of sticky nanotubes. *Science* **2005**, *309*, 920–923.
- (3) Gabriel, J.-C. P.; Davidson, P. New trends in colloidal liquid crystals based on mineral moieties. *Adv. Mater.* **2000**, *12*, 9–20.
- (4) Hobbie, E. K.; Fry, D. J. Nonequilibrium phase diagram of sticky nanotube suspension. *Phys. Rev. Lett.* **2006**, *97*, 036101.
- (5) Siró, I.; Plackett, D. Microfibrillated cellulose and new nanocomposite materials: A review. *Cellulose* **2010**, *17*, 459–494.
- (6) De Souza Lima, M. M.; Borsali, R. Rodlike cellulose microcrystals: Structure, properties, and applications. *Macromol. Rapid Commun.* **2004**, *25*, 771–787.
- (7) Solomon, M. J.; Spicer, P. T. Microstructural regimes of colloidal rod suspensions, gels, and glasses. *Soft Matter* **2010**, *6*, 1391.
- (8) Barry, E.; Beller, D.; Dogic, Z. A model liquid crystalline system based on rodlike viruses with variable chirality and persistence length. *Soft Matter* **2009**, *5*, 2481–2668.
- (9) Dennison, M.; Dijkstra, M.; van Roij, R. Phase diagram and effective shape of semiflexible colloidal rods and biopolymers. *Phys. Rev. Lett.* **2011**, *106*, 208302.
- (10) Vroege, G. J.; Lekkerkerker, H. N. W. Phase transitions in lyotropic colloidal and polymer liquid crystals. *Rep. Prog. Phys.* **1992**, *55*, 1241–1309.
- (11) Geyer, U.; Heinze, T.; Stein, A.; Klemm, D.; Marsch, S.; Schumann, D.; Schmauder, H. P. Formation, derivatization and applications of bacterial cellulose. *Int. J. Biol. Macromol.* **1994**, *16*, 343–347.
- (12) Kuijk, A.; Koppert, R.; Versluis, P.; Nijse, J.; Velikov, K. P. Dispersions of attractive semi-flexible fiberlike colloidal particles from bacterial cellulose microfibrils. *Langmuir* **2013**, *29*, 14356–14360.
- (13) Lee, K.-Y.; Quero, F.; Blaker, J. J.; Hill, C. A. S.; Eichhorn, S. J.; Bismarck, A. Surface only modification of bacterial cellulose nanofibres with organic acids. *Cellulose* **2011**, *18*, 595–605.
- (14) Saito, T.; Hirota, M.; Tamura, N.; Kimura, S.; Fukuzumi, H.; Heux, L.; Isogai, A. Individualization of nano-sized plant cellulose fibrils by direct surface carboxylation using TEMPO catalyst under neutral conditions. *Biomacromolecules* **2009**, *10*, 1992–1996.
- (15) Saito, T.; Nishiyama, Y.; Putaux, J.-L.; Vignon, M.; Isogai, A. Homogeneous suspensions of individualized microfibrils from TEMPO-catalyzed oxidation of native cellulose. *Biomacromolecules* **2006**, *7*, 1687–1691.
- (16) Sorvari, A.; Saarinen, T.; Haavisto, S.; Salmela, J.; Vuoriluoto, M.; Seppälä, J. Modifying the flocculation of microfibrillated cellulose suspensions by soluble polysaccharides under conditions unfavorable to adsorption. *Carbohydr. Polym.* **2014**, *106*, 283–292.
- (17) Yamamoto, H.; Horii, F. In situ crystallization of bacterial cellulose I. Influences of polymeric additives, stirring and temperature on the formation celluloses Ia and Ib as revealed by cross polarization/magic angle spinning (CP/MAS) <sup>13</sup>C NMR spectroscopy. *Cellulose* **1994**, *1*, 57–66.
- (18) Haigler, C. H.; White, A. R.; Brown, R. M.; Cooper, K. M. Alteration of in vivo cellulose ribbon assembly by carboxymethylcellulose and other cellulose derivatives. *J. Cell Biol.* **1982**, *94*, 64–69.
- (19) Versluis, P.; Popp, A. K.; Velikov, K. P. Interaction between biopolyelectrolytes and sparingly mineral particles. *Langmuir* **2011**, *27*, 83.
- (20) Pusey, P. N.; van Megen, W. Dynamic light scattering by non-ergodic media. *Phys. A* **1989**, *157*, 705–741.

- (21) Kroon, M.; Wegdam, G. H.; Sprik, R. Dynamic light scattering studies on the sol–gel transition of a suspension of anisotropic colloidal particles. *Phys. Rev. E: Stat. Phys., Plasmas, Fluids, Relat. Interdiscip. Top.* **1996**, *54*, 6541–6550.
- (22) Berne, B. J.; Pecora, R. *Dynamic Light Scattering*; John Wiley and Sons, Inc.: Hoboken, NJ, 2000.
- (23) Buining, P. A.; Philipse, A. P.; Lekkerkerker, H. N. W. Phase behavior of aqueous dispersions of colloidal boehmite rods. *Langmuir* **1994**, *10*, 2106–2114.
- (24) Gabriel, J. P.; Sanchez, C.; Davidson, P. Observation of nematic liquid-crystal textures in aqueous gels of smectite clays. *J. Phys. Chem.* **1996**, *100*, 11139–11143.
- (25) Mourad, M. C. D.; Byelov, D. V.; Petukhov, A. V.; Lekkerkerker, H. N. W. Structure of the repulsive gel/glass in suspensions of charged colloidal platelets. *J. Phys.: Condens. Matter* **2008**, *20*, 494201.
- (26) Mourad, M. C. D.; Wijnhoven, J. E. G. J.; Van't Zand, D. D.; van der Beek, D.; Lekkerkerker, H. N. W. Gelation versus liquid crystal phase transitions in suspensions of plate-like particles. *Philos. Trans. R. Soc., A* **2006**, *364*, 2807–2816.
- (27) Pelletier, O.; Davidson, P.; Bourgaux, C.; Livage, J. The effect of attractive interactions on the nematic order of  $V_2O_5$  gels. *Europhys. Lett.* **1999**, *48*, 53–59.
- (28) Kerekes, R. J. Rheology of fibre suspensions in papermaking—An overview of recent research. *Nord. Pulp Pap. Res. J.* **2006**, *21*, 598–612.
- (29) Liimatainen, H.; Haavisto, S.; Haapala, A.; Niinimäki, J. Influence of adsorbed and dissolved carboxymethyl cellulose on fibre suspension dispersion, dewaterability, and fined retention. *BioResources* **2009**, *4*, 321–340.
- (30) Eronen, P.; Junka, K.; Laine, J.; Österberg, M. Interaction between water-soluble polysaccharides and native nanofibrillar cellulose thin films. *BioResources* **2011**, *6*, 4200–4217.
- (31) Laine, J.; Lindström, T. Studies on topochemical modification of cellulosic fibres. Part 1. Chemical conditions for the attachment of carboxymethyl cellulose onto fibres. *Nord. Pulp Pap. Res. J.* **2000**, *15*, 520–526.
- (32) Manning, G. S. Counterion condensation on charged spheres, cylinders, and planes. *J. Phys. Chem. B* **2007**, *111*, 8554–8559.
- (33) Myllytie, P.; Holappa, S.; Paltakari, J.; Laine, J. Effect of polymers on aggregation of cellulose fibrils and its implication on strength development in wet paper web. *Nord. Pulp Pap. Res. J.* **2009**, *24*, 125–134.
- (34) Fall, A. B.; Lindström, S. B.; Sundman, O.; Ödberg, L.; Wågberg, L. Colloidal stability of aqueous nanofibrillated cellulose dispersions. *Langmuir* **2011**, *27*, 11332–11338.
- (35) Wågberg, L.; Decher, G.; Norgren, M.; Lindström, T.; Ankerfors, M.; Axnäs, K. The build-up of polyelectrolyte multilayers of microfibrillated cellulose and cationic polyelectrolytes. *Langmuir* **2008**, *24*, 784–795.
- (36) Safari, S.; Sheikhi, A.; van de Ven, T. G. M. Electroacoustic characterization of conventional and electrosterically stabilized nanocrystalline celluloses. *J. Colloid Interface Sci.* **2014**, *432*, 151–157.
- (37) Khaled, B.; Abdelbaki, B. Rheological and electrokinetic properties of carboxymethylcellulose–water dispersions in the presence of salts. *Int. J. Phys. Sci.* **2012**, *7*, 1790–1798.
- (38) Van Bruggen, M. P. B.; Lekkerkerker, H. N. W. Metastability and multistability: Gelation and liquid crystal formation in suspensions of colloidal rods. *Langmuir* **2002**, *18*, 7141–7145.
- (39) Heux, L.; Chauve, G.; Bonini, C. Nonfloculating and chiral-nematic self-ordering of cellulose microcrystals suspensions in nonpolar solvents. *Langmuir* **2000**, *16*, 8210–8212.
- (40) Orts, W. J.; Godbout, L.; Marchessault, R. H.; Revol, J.-F. Enhanced ordering of liquid crystalline suspensions of cellulose microfibrils: A small angle neutron scattering study. *Macromolecules* **1998**, *31*, 5717–5725.
- (41) Gousse, C.; Chanzy, H.; Excoffier, G.; Soubeyrand, L.; Fleury, E. Stable suspensions of partially silylated cellulose whiskers dispersed in organic solvents. *Polymer* **2002**, *43*, 2645–2651.
- (42) Huang, F.; Rotstein, R.; Fraden, S.; Kasza, K. E.; Flynn, N. T. Phase behavior and rheology of attractive rod-like particles. *Soft Matter* **2009**, *5*, 2766.
- (43) Onsager, L. The effects of shape on the interactions of colloidal particles. *Ann. N. Y. Acad. Sci.* **1949**, *51*, 627–659.
- (44) Sun, C. True density of microcrystalline cellulose. *J. Pharm. Sci.* **2005**, *94*, 2132–2134.
- (45) Vroege, G. J. The isotropic–nematic phase transition and other properties of a solution of semi-flexible polyelectrolytes. *J. Chem. Phys.* **1989**, *90*, 4560–4566.
- (46) Van den Pol, E.; Thies-Weesie, D. M. E.; Petukhov, A. V.; Kvashnina, K.; Vroege, G. J. Influence of polydispersity on the phase behavior of colloidal goethite. *J. Chem. Phys.* **2008**, *129*, 164715.
- (47) Tzoumaki, M. V.; Moschakis, T.; Biliaderis, C. G. Metastability of nematic gels made of aqueous chitin nanocrystal dispersions. *Biomacromolecules* **2010**, *11*, 175–181.
- (48) Habibi, Y.; Chanzy, H.; Vignon, M. R. TEMPO-mediated surface oxidation of cellulose whiskers. *Cellulose* **2006**, *13*, 679–687.
- (49) Montanari, S.; Roumani, M.; Heux, L.; Vignon, M. R. Topochemistry of carboxylated cellulose nanocrystals resulting from TEMPO-mediated oxidation. *Macromolecules* **2005**, *38*, 1665–1671.